communications physics

Article

https://doi.org/10.1038/s42005-024-01683-w

Density profile of ^{3}He in a nanoscale ^{3}He-^{4}He superfluid film determined by neutron scattering

Oleg Kirichek [1] ✉, Christopher R. Lawson[1], Christy J. Kinane [1], Andrew J. Caruana [1], Sean Langridge [1], Timothy R. Charlton [2] & Peter V. E. McClintock [3]

For decades, superfluid helium has attracted the interest of the scientific community as an extremely pure realisation of a quantum liquid, only accessible at temperatures close to absolute zero. Previously, helium films have only been observed directly using X-rays. However, this method is limited to temperatures above 1 K due to the high levels of energy deposition, and it also suffers from an inability to distinguish between helium isotopes. Here we show that a ^{3}He layer on top of a phase separated mixture film at 170 mK gradually dissolves into the ^{4}He with increasing temperature. We also observe an anomaly in film behaviour near 300 mK and unexpected restoration of the layered structure at 1.5 K which is consistent with a re-entrant phase transition leading to the suppression of superfluidity in the film near 300 mK. Our successful application of neutron scattering to study helium films at ultra-low temperatures opens up new possibilities for future research.

The discovery of superfluidity in ^{4}He heralded a new age of research into macroscopic quantum phenomena. Of the many strange effects witnessed in superfluids at low temperatures, those in thin films remain among the most elusive for experimental investigation. A thin film of highly mobile helium coats all surfaces whose lower extremities touch the superfluid, except for certain alkali metals[1]. Superfluid films host a variety of iconic quantum phenomena, such as the Kosterlitz–Thouless topological phase transition[2], Rollin film flow[3], and third sound[4] including the existence of a critical Casimir force between the interfaces of the film, near the ^{3}He–^{4}He tricritical point[5] and the superfluid transition[6]. Superfluid helium films have the potential for important applications in quantum optomechanics[7,8].

The addition of ^{3}He to superfluid ^{4}He allows us to observe and study phase-separated ^{3}He/^{4}He mixture films below 1K[9,10]. Because the liquid ^{4}He isotope obeys Bose–Einstein statistics, whereas ^{3}He is governed by Fermi statistics, a ^{3}He–^{4}He mixture facilitates experimental studies of the interplay between these two fundamental quantum statistics.

More than 50 years ago, Andreev showed that ^{3}He atoms are bound to the free surface of ^{4}He[11]. The most important development in the study of mixture films has been the understanding of ^{3}He impurity energetics in a ^{4}He environment[9,10]. Below 150 mK, ^{3}He–^{4}He mixture films exhibit nearly complete phase separation[12] with a lower (i.e. closer to the substrate) layer of mainly superfluid ^{4}He, and a thin upper layer of ^{3}He–^{4}He mixture[13]. In the zero temperature limit, the ^{3}He is in its ground state, which in physical space is located on the surface of the ^{4}He film[10]. As the temperature increases, ^{3}He will be promoted into higher energy states, leading to the mixing of ^{3}He into the ^{4}He film[10,14,15].

Particle beam experiments have allowed some insight into the behaviour of thin helium films. X-ray specular reflectometry enables the measurement of the depth and surface profiles of ^{4}He films adsorbed onto silicon substrates[16,17]. However, this method is limited to temperatures above 1 K due to the high levels of energy deposition[18]. Furthermore, the technique is unable to distinguish between the ^{3}He and ^{4}He isotopes, which is a significant distinction in the study of ^{3}He–^{4}He mixture films[19].

The weak interaction of neutrons with matter substantially reduces the problem of overheating that arises with particle or X-ray beams, thus allowing neutron scattering experiments down into the millikelvin temperature range[20,21]. Furthermore, the two helium isotopes have very different neutron scattering cross-sections[22] (see Table 1), as well as very different absorption cross sections, thus enabling their contributions to be separated. Indeed, the strong absorption cross-section of ^{3}He has made it the mainstay of neutron detectors for decades[23] and also allows neutron imaging of the separate helium isotopes via neutron radiography[24]. This has enabled inelastic neutron scattering observations of surface ripplon excitations in atomically thick liquid ^{4}He[20] and, more recently, observation of roton-like excitations in a ^{3}He monolayer[21]. A comprehensive review of neutron scattering studies of atomic thickness ^{3}He films is given in[25]. Whilst there exists a significant body of work on low-temperature helium mixture films, for a variety of ^{3}He concentrations, their focus is on much thinner films[9].

[1]ISIS Neutron and Muon Source, Rutherford Appleton Laboratory, Harwell Science and Innovation Campus, Oxon OX11 0QX, UK. [2]Neutron Sciences Division, Oak Ridge National Laboratory, Oak Ridge, TN 37831, USA. [3]Department of Physics, Lancaster University, Lancaster LA1 4YB, UK. ✉e-mail: oleg.kirichek@stfc.ac.uk

Here we have investigated a thicker saturated helium film with a thickness of about 45 atomic layers: our results may not be applicable to unsaturated helium films.

Our earlier experiments on specular neutron reflection from the surface of bulk liquid ^{3}He–^{4}He mixtures[26,27] were complicated and ultimately frustrated by departures of the liquid surface from optical flatness and, in particular, those associated with its meniscus spreading from the wall of the container. Another serious problem was that mechanical vibrations could easily disturb the bulk liquid helium surface. Here, we use a silicon block as a film substrate, with the bulk helium surface tens of millimetres below, thereby eliminating the meniscus problem. This arrangement also increases the surface area available for neutron reflection, and it improves the film's stability in the face of helium surface distortions caused by vibrations. The mechanical vibrations of the sample are mostly displacements where the silicon block moves as a whole, together with the helium film.

Table 1 | The scattering properties of the helium isotopes in the solid and liquid states at a temperature of 1 K[58,59]

Isotope	*b* (fm)	Density (g/cm^3)	nSLD (×10^{-6} Å^{-2})
^{3}He @ 1K	5.74-1.483i	0.08172	0.9366
^{4}He @ 1K	3.26	0.14511	0.7117
Solid ^{4}He	3.26	0.187	0.9172

b is the bound coherent scattering length in femtometres (fm)[22]. nSLD is the scattering length density defined as the product *Nb* where *N* is the number density of the material in question in atoms per Å^3[19,22]. Note the large imaginary component of *b* for ^{3}He, indicating its large absorption cross section for neutrons, a feature that is absent for ^{4}He. ^{4}He and ^{3}He scattering length densities as a function of temperature are presented in Supplementary Note 1.

Here we report an ultra-low-temperature experimental investigation of saturated, van der Waals superfluid helium films based on neutron reflectivity. We study a liquid ^{4}He sample of commercial purity (containing about 2×10^{-7} of ^{3}He) and a 0.1% ^{3}He–^{4}He mixture. Thanks to the exceptional sensitivity and precision of neutron reflectivity, we can observe and study a 160 Å thick superfluid helium film on the silicon surface. We have observed a phase-separated ^{3}He/^{4}He mixture film at 170 mK, and have been able to watch the gradual dissolution of its ^{3}He top layer into the ^{4}He with increasing temperature. We have also observed an anomaly in the film's behaviour near 300 mK and have discovered an unexpected restoration of the layered structure at 1.5 K.

Results

Neutron reflectivity curves

In Fig. 1a, c, we present normalised reflectivity curves for the nominally pure ^{4}He film, which had a ^{3}He/^{4}He ratio of ^{3}He ~ 10^{-7} (commercial helium), compared with results from a 0.1% of ^{3}He in ^{4}He mixture. The red curves show the reflectivity signal from the bare surface of the silicon substrate obtained in a separate measurement. The nominally pure ^{4}He data were collected at 150 mK and the mixture data at 170 mK. The reflectivity for the pure ^{4}He and the mixture differ significantly. In each case, the deviations in reflectivity from that of the bare substrate indicate unambiguously the formation of a layered structure, as shown by the presence of Kiessig fringes[28,29]. Kiessig fringes arise due to constructive and destructive interference of the incoming and outgoing neutrons as they reflect from the film surface and the substrate/film (bottom-most) interface. This means they provide information on the total thickness of the film and indicate the presence of a thin film of helium. From the reflectivity data, we can extract the full spatial variation of the scattering length density through the film via an iterative fitting process. The experimental data were analysed using the

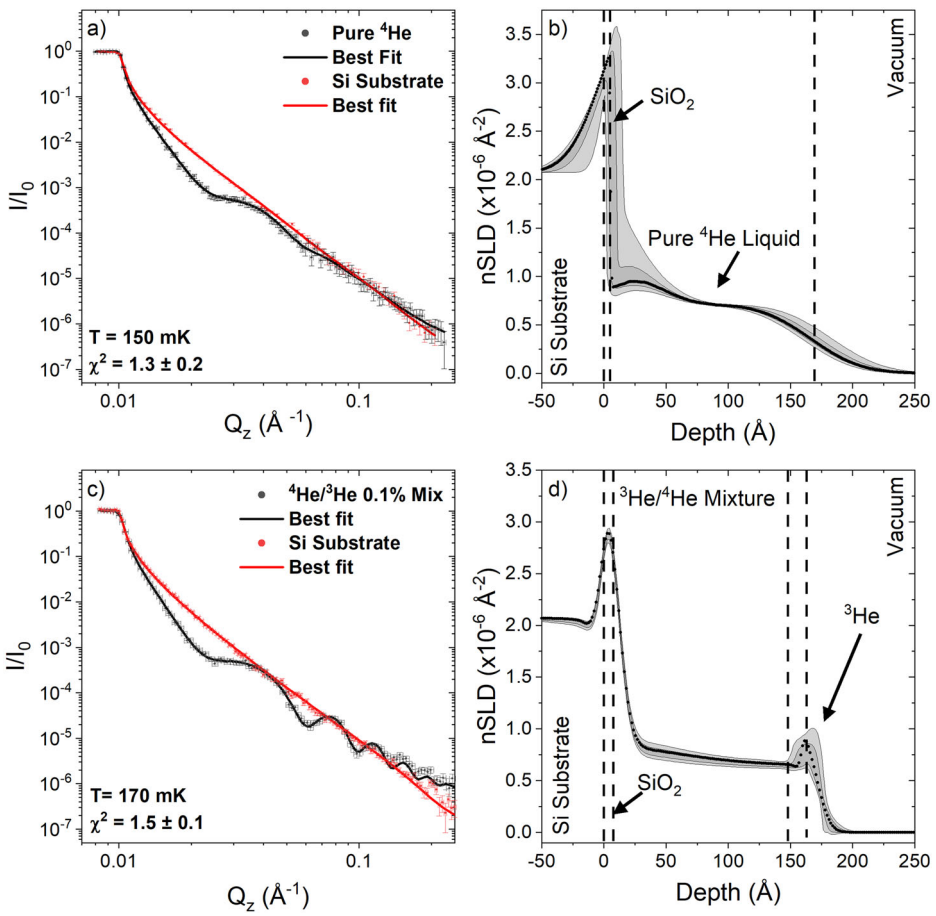

Fig. 1 | Reflectivity curves and neutron scattering length density profiles for nominally pure ^{4}He and for the ^{3}He–^{4}He mixture. a The reflectivity curve for the nominally pure ^{4}He film. **b** The neutron scattering density profiles for pure ^{4}He. **c** The reflectivity curve for the 0.1% of ^{3}He in ^{4}He mixture. **d** The neutron scattering density profiles for the helium mixture. Q_z is the out-of-plane wavevector transfer and I/I_0 is the detected intensity, I, normalised to the incident intensity, I_0, also referred to as the reflectivity. The red curves show the reflectivity signal from the bare surface of the silicon substrate, measured separately. The solid lines represent the best fit to the data. The black dotted line is the nSLD profile derived from the best fit to the data. The grey regions (dark and light) represent the 1σ (68%) and 2σ (95%) Bayesian confidence intervals respectively. χ^2 is the conventional measure of the goodness-of-fit and indicates excellent agreement with the data.

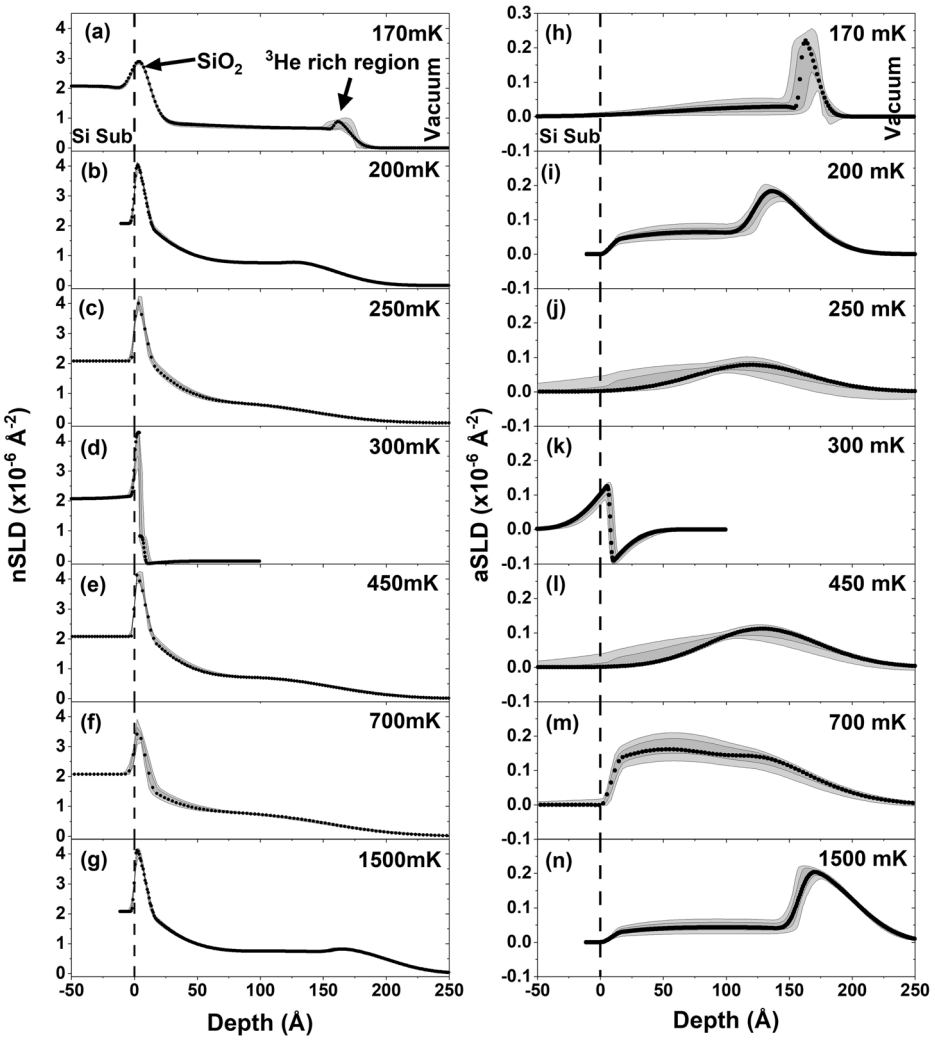

Fig. 2 | Nuclear scattering length density (nSLD) profiles and neutron adsorption scattering length density (aSLD) profiles. a–g nSLD profiles. **h–n** aSLD profiles. Measurements are shown at temperatures of 170, 200, 250, 300, 450, 700 and 1500 mK. In the ^{3}He/^{4}He mixture film almost all absorption occurs due to the ^{3}He atoms. The absorption (aSLD) curves, therefore, give a good representation of the distribution of ^{3}He atoms inside the film.

Refl1D software package[30]. Details of the analysis are given in Supplementary Notes 2–4.

Neutron scattering density profiles

In Fig. 1b, d, we present the nuclear neutron scattering density (nSLD) profiles resulting from the data analyses for the pure ^{4}He and the helium mixture, respectively. The nominal bulk nSLD profiles are given in Table 1. In both cases, as we move away from the surface of the substrate, the scattering density plateaus out at a value corresponding approximately to the scattering density of liquid ^{4}He. The main difference between the two profiles is the existence of a density anomaly (^{3}He) at the surface of the helium mixture film. Qualitatively, this layer provides additional neutron contrast resulting in an enhancement of the Kiessig fringes. For the ^{3}He–^{4}He mixture there is a small enhancement of the Kiessig fringes due to the enhanced contrast of the ^{3}He at the surface. For pure ^{4}He there is also a slightly more pronounced increase in nSLD at the SiO_2 interface that is indicative of the formation of a thin solid ^{4}He layer[16,17]. The grey bands in Fig. 2b, d represents the 1σ and 2σ Bayesian confidence intervals on the reflectivity analysis. Both the reflectivity curve and density profile of pure ^{4}He exhibits little change between 150 mK and 1.5 K. The complete set of reflectivity curves are presented in the Supplementary Fig. 11. The minor changes observed could be attributable to the temperature dependence of the ^{4}He surface tension. The peak positioned at the surface of the silicon substrate in both cases is caused by a native SiO_2 layer. It should be noted that all the helium interfaces, especially in the pure ^{4}He case, are rough/diffuse. A possible explanation lies in the effect of mechanical vibrations generated by the pulse-tube cryo-cooler of the dilution refrigerator. After obtaining initial results of the kind shown in Fig. 1b, we implemented several anti-vibration measures, such as moving the pulse tube motor to a remote location suspended by flexible mounts and similarly isolating the dilution fridge pumping lines. This substantially reduced the amplitude of vibrations and consequently improved the spatial resolution. This change can be seen in the sharpness of the vacuum-He interface as shown in Fig. 1d.

We now turn to the temperature evolution of the ^{3}He–^{4}He mixture. In Fig. 2 we show the evolution of the nSLD profile of the 0.1% ^{3}He/^{4}He mixture film during warming. At 170 mK, panel (a), most of the ^{3}He is concentrated in a narrow band at the surface of the helium film[9,12]. This is confirmed by the absorption scattering length density plot (aSLD) shown in panel (h); it should be noted that only the ^{3}He significantly absorbs neutrons, so the aSLD plots give a good measure of where the ^{3}He is situated within the film.

As the temperature increases to 200 mK, panel (b), ^{3}He begins to dissolve into the ^{4}He[9,10] as can be seen by the broadening of features in the aSLD in panel (i). At 250 mK, panels (c and j), film stratification has disappeared. A very striking and unexpected change occurs at 300 mK, panels (d) and (k), where the profile is essentially just that of the Si substrate alone. It is as though the film has largely disappeared. There is, however, evidence for a thin absorbing layer that is not present either for the bare Si substrate or for the Si plus film at other temperatures. These changes are reversible: cooling to 170 mK restored the stratification, with both profiles recovering their original form; increasing the temperature back to 300 mK again reproduced the same result as observed previously. At 450 mK, however, in

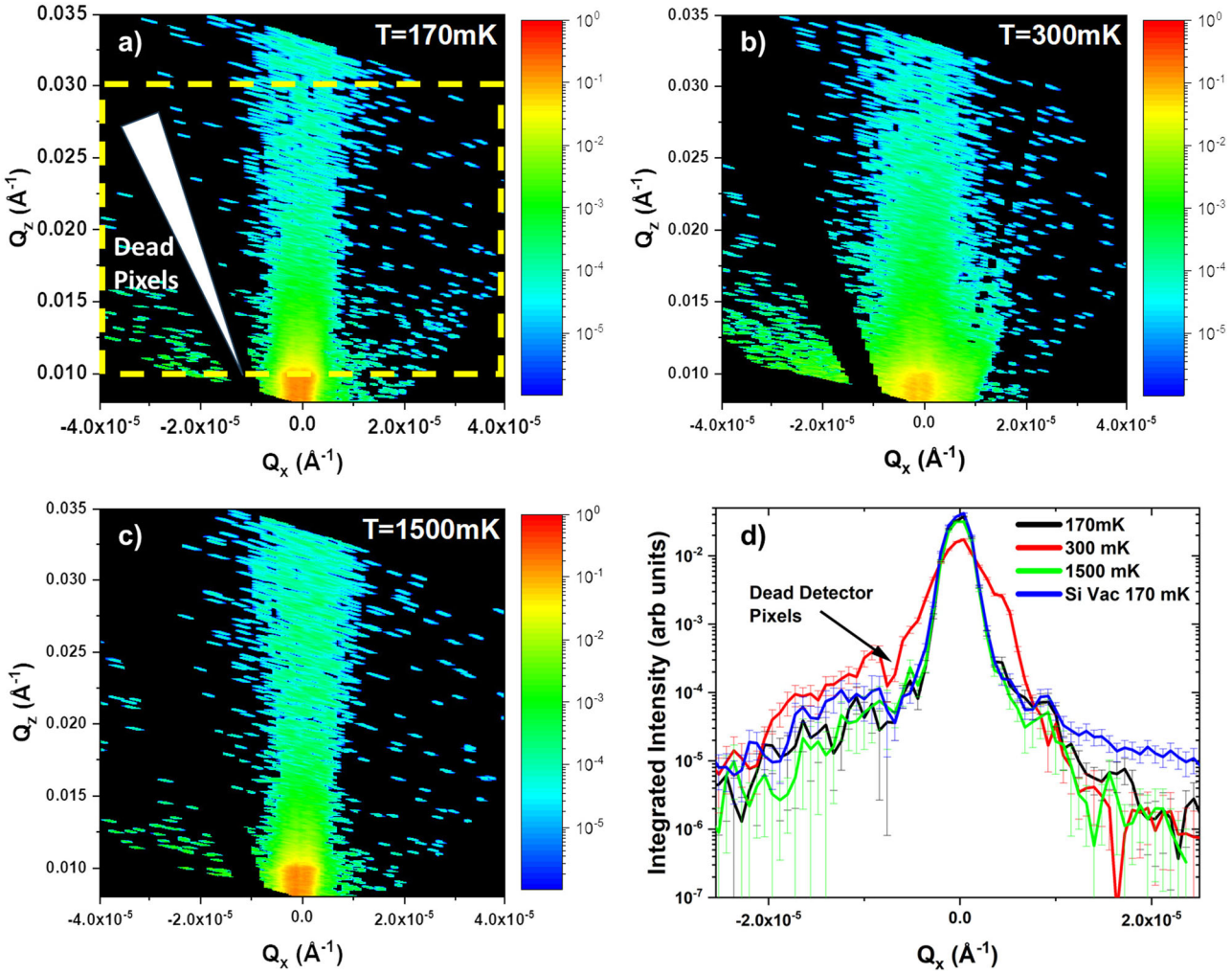

Fig. 3 | Specular and off-specular neutron scattering from the ^{3}He/^{4}He mixture for three different temperatures. Q_z is the out-of-plane wavevector transfer and Q_x is the in-plane wavevector transfer. The intensity colour scale is logarithmic and shows the I/I_0 reflectivity for three different temperatures: 170 mK (**a**), 300 mK (**b**) and 1500 mK (**c**). The high-intensity critical edge can be seen for $Q_x \approx 0$, $Q_z \leq 0.01$ Å^{-1}. There is a significant rise in the off-specular scattering at 300 mK and low Q_z (**b**). This is highlighted in the pseudo rocking curves displayed in (**d**), where the 170 mK, 1500 mK and Si-only curves have essentially the same width, but the 300 mK curve is noticeably broader. These pseudo rocking curves were created by integrating constant lines in the Q_z direction over the Q_z range 0.01–0.03 Å^{-1} as shown by the yellow-dashed box in (**a**) and are intended to highlight the changes in the reciprocal space maps rather than provide a quantitative analysis. The dead zone on the left of each image is due to the masking of several dead detector pixels in the time of flight maps when converted to reciprocal space maps. This appears as an averaged-out dip in the pseudo-rocking curves.

panel (e), the film re-formed on the silicon surface, with a profile similar to that at 250 mK. At 700 mK, panel (f), the ^{3}He distribution in the film has become more homogeneous. At 1.5 K the film unexpectedly returned to its stratified form, similar to that at 200 mK, with ^{3}He predominantly remaining close to the surface of the slightly thicker film. For all temperatures, except 300 mK, the data are accurately described by the same parameterised model. This is not the case, however, for the 300 mK data where the best fit required a very thin inhomogeneous layer rich in ^{3}He on the substrate. This result was unexpected and was, to say the least, highly unusual.

Off-specular neutron scattering maps

Exploration of the nature of this effect required the use of off-specular neutron scattering ($Q_X \neq 0$) to provide information about in-plane structure/correlations. The POLREF reflectometer collects this information via its position-sensitive detector. In Fig. 3 we show the off-specular maps from the mixture as a function of temperature. $Q_x = 0$ is the true specular reflectivity which is typically broadened by instrumental resolution and in-plane inhomogeneities of the sample. If there are no changes in the in-plane correlations, the width of this ridge of scattering will remain constant. In Fig. 3b, we see a significant rise in off-specular scattering at around 300 mK for low Q_z close to the critical reflection edge. Particularly at low Q_z, the scattering increases in width before decreasing back to its resolution-limited width at all other temperatures. An analysis of the first Kiessig fringe shown in Supplementary Note 5 indicates that the specular ridge does not change in width as would be expected if the surface of the film were roughening in the plane of the film. The observed scattering at lower Q_z near the critical edge is similar to Yoneda scattering[31] which can result from non-correlated roughness. The scattering would be consistent with height-height fluctuations with an in-plane correlation length (cut-off) of the order of microns or possibly a rupturing of the film. Pseudo-rocking curves created, near the critical edge, shown in panel (d), qualitatively show the change at 300 mK much more clearly. It is evident how similar the peaks at 170 mK, 1500 mK and the bare silicon curves are. The pseudo-rocking curves were created by integrating constant lines in the Q_z direction over the Q_z range from 0.01–0.03 Å^{-1} as shown by the dashed yellow box in panel (a). The reciprocal space map for the Silicon-only case is shown in the Supplementary Note 3.

Discussion

The difference in the neutron scattering properties of the ^{4}He and ^{3}He isotopes has allowed us to observe directly the ^{3}He–^{4}He mixture film phase separation at 170 mK[12]. The expected mixing ^{3}He into the mainly ^{4}He film with increasing temperature[14,15] was clearly demonstrated.

Krotscheck et al.[10] developed a microscopic theory to describe the system of ^{3}He atoms adsorbed on the surface of a liquid ^{4}He film. To avoid instability at finite wave numbers due to the formation of a solid layer close to the substrate, they weakened the short-range attraction and adjusted the attractive tail of the potential to a value about midway between the experimental and the theoretically predicted[32] values. Their calculations gave the energy difference between the ground and the first excited states as 1.52 K, and that between the ground and the second excited states as 2.75 K, for 0.30 Å^2 surface coverage[10]. These results agree with the experimental value of 2.28 K for the ^{3}He binding energy obtained from "surface sound" experiments on helium mixture films[14]. The calculations were performed for four surface coverages, with the largest, 0.30 Å^2, corresponding to a 15 Å ^{4}He film thickness. However, the authors expected that their calculation for the thickest film is representative of the limit of an infinite half-space. Thus the theory can appropriately be compared with our experimental results for a 160 Å thick helium film.

The results in Fig. 2 show that, at the lowest temperature of 170 mK, almost all of the ^{3}He stays close to the free surface of the helium film. As temperature increases, ^{3}He atoms leave the surface and dissolve into the bulk of the film. At 250 mK the stratification almost disappears. The temperature scale of this transformation agrees well with the theoretical results of Ref. 10. The absence of ^{3}He states near a strongly binding substrate is demonstrated by our experiment, as no ^{3}He impurity-bound states are observed near the silicon substrate, consistent with the theoretical prediction[33] and experimental results for strong-bonding substrates[34].

Our most intriguing observation is the dramatic transition in the ^{3}He–^{4}He mixture film at 300 mK. The scattering density and neutron absorption profiles in Fig. 2 demonstrate the absence of a homogeneous helium film, and the generation of disorder on the substrate surface that we postulate may consist of a quasi-layer that must contain some ^{3}He, as it is the only element in the system that absorbs sufficiently to give this level of effect. We note that the Si substrate alone shows no evidence of off-specular scattering at low temperature indicating that it is the layer that is producing the additional scattering.

As the temperature rises, ^{3}He mixes into the main superfluid ^{4}He film. The occupation of higher energy states by ^{3}He atoms may lead to a suppression of superfluidity at around 300 mK, accompanied by density fluctuations. As discussed in[35], adding a small amount of ^{3}He destabilises the film, so these fluctuations could easily disrupt an already unstable film. One might also expect that critical Casimir forces[6] could affect the film thickness and stability as the film goes through a superfluid transition. Another possible mechanism could be film instability in the vicinity of a phase transition, caused by the short-range repulsive potential on those substrates whose electrons are weakly bound and extend far outward from the surface. This phenomenon has been studied for alkali metal surfaces[36] but, hypothetically, might also arise in the case of surface charges trapped in the silicon oxide layer. Further neutron reflectivity measurements, particularly off-specular ones, will be required for a deeper understanding of this phenomenon.

At 450 mK the film reappears as a homogeneous, structureless helium mixture film and remains in this state up to 700 mK. The marked change in the structure of the film at 300 mK, and the fact that its structure is similar both below and above this temperature, suggest the existence of a re-entrant phase transition close to 300 mK.

The restoration of enhanced fringes at 1.5 K is another quite unexpected result. Similarly to the 300 mK anomaly, the film undergoes significant structural changes between 700 mK and 1.5 K. At these temperatures the vapour pressure of both helium isotopes becomes non-negligible, which complicates the situation further. Significant amounts of ^{3}He and ^{4}He in the vapour phase mean that the precise isotopic concentration in the film unknown and in a constant state of flux. This feature tempts us to speculate that there might be a second, "high temperature" phase transition, perhaps as discussed in[37–39]. However, the current experimental data are insufficient to draw a definitive conclusion about either the existence or the nature of this transition.

The role of quantised vortices in the film should also be considered. Vortices are known to trap ^{3}He in their cores at very low temperatures[40–42]. As the temperature rises, the ^{3}He starts to be released at a critical temperature that depends on the isotopic concentration, occurring at about 0.5 K for a 0.1% bulk solution[40]. Could this process be responsible for the anomaly in the neutron reflectivity that we observe near 0.3 K? It is likely that some vortices will indeed exist in the film. These can be remanent vortices[43] in the bulk superfluid, created when the nascent superfluid film wets the Si substrate, or created through vibrations transmitted from the pulse tube of the refrigerator. To have a significant effect on the distribution of the ^{3}He in a film, however, their density would need to be high enough to compete with the surface states in attracting ^{3}He. We may speculate that the absorption of ^{3}He into surface states might effectively reduce the ^{3}He concentration of the solution, thereby driving the vortices' absorption/desorption transition lower in temperature. To our knowledge, however, there is no evidence for the required high density of quantised vortices existing in superfluid films. We conclude that, although there is probably some trapping and release of ^{3}He from vortices in the film, the effect is unlikely to be of significance in the present context.

Looking to the future, we note that the use of polarised neutrons and a magnetic reference layer[44,45] would yield even greater sensitivity to the observed separation of the helium isotopes. The extremely low level of neutron beam heating, combined with the high isotopic sensitivity of neutron scattering, promises to reignite interest in the search for superfluidity in 2D ^{3}He films[46], in the 2D Fermi liquid-gas transition proposed by Andreev and Kompaneets[47], and in the study of helium surface excitations in the ultra-low temperature limit[48]. An understanding of helium film properties is also important for the development of qubits based on the surface electrons on helium[49,50]. It could also contribute to dilution refrigerator development, e.g. of the powerful machines needed for cooling quantum computers whose performance is currently limited by helium film effects. A better understanding of the latter could lead to enhanced cooling power.

In summary, we have presented a study of pure ^{4}He and ^{3}He/^{4}He mixture films using specular neutron reflection, in the temperature range of 150 mK to 1.5 K. Thanks to the exceptional sensitivity and precision of this technique, we have observed a phase-separated ^{3}He/^{4}He mixture film at 170 mK, and have been able to watch the gradual dissolution of its ^{3}He top layer into ^{4}He with increasing temperature, in agreement with current theories[10,14,15]. Furthermore, the surprising behaviour of the helium mixture at 300 mK hints at the possibility of an as-yet unstudied geometrically restricted phase transition. The subsequent restoration of the layered structure at 1.5 K was equally unexpected.

Methods

Sample environment: dilution refrigerator

The experiment was undertaken using the cryogen-free dilution refrigerator E-18, manufactured by Oxford Instruments. This refrigerator has an unloaded base temperature of around 20mK, with a cooling power of 300 μW at 100 mK. The cell is attached via a copper bracket to the mixing chamber of the dilution refrigerator, which is itself mounted on the positioning table of the Time of Flight (ToF) neutron reflectometry instrument POLREF[51] at the ISIS neutron and muon source. Connection to the interior of the cell was made using an indium-sealed joint that allowed helium to be dosed into the cell via thin-walled capillaries. These capillaries were well-thermalised at each of the refrigerator's cooling stages using copper bobbins.

To reduce the level of vibration in the equipment, caused by the pulse tube cooler of the cryogen-free dilution refrigerator, it features some degree of mechanical detachment from the pulse tube in the form of copper braids. The motor head that drives the cooler is also remotely mounted some

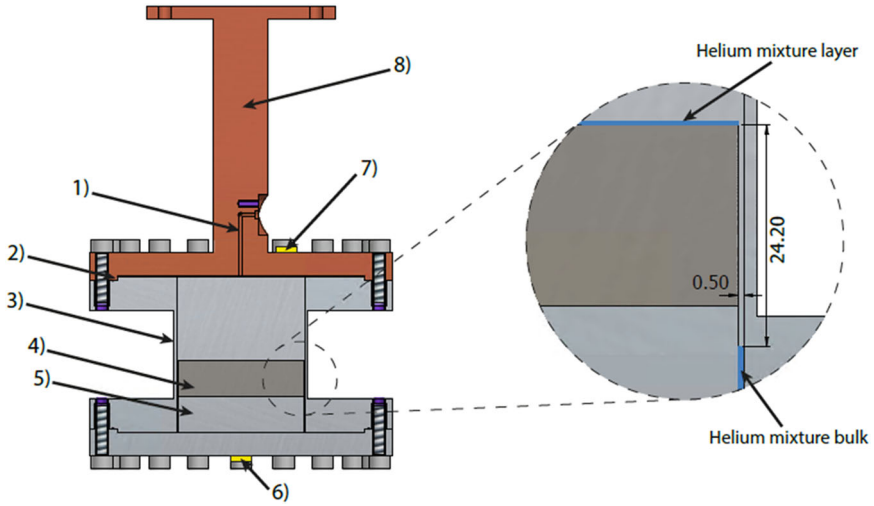

Fig. 4 | The experimental cell used for this study. The schematic shows the experimental cell where: (1) is the cell fill line; (2) Indium joint; (3) thin Aluminium (7075-T6) cell wall; (4) treated silicon block; (5) aluminium support block; (6) resistive heater; (7) calibrated RuO_2 thermometer; (8) copper bracket, connected to mixing chamber of dilution fridge. The enlarged section on the right shows the positions of the horizontal part of the helium film and the surface of bulk helium liquid with essential dimensions.

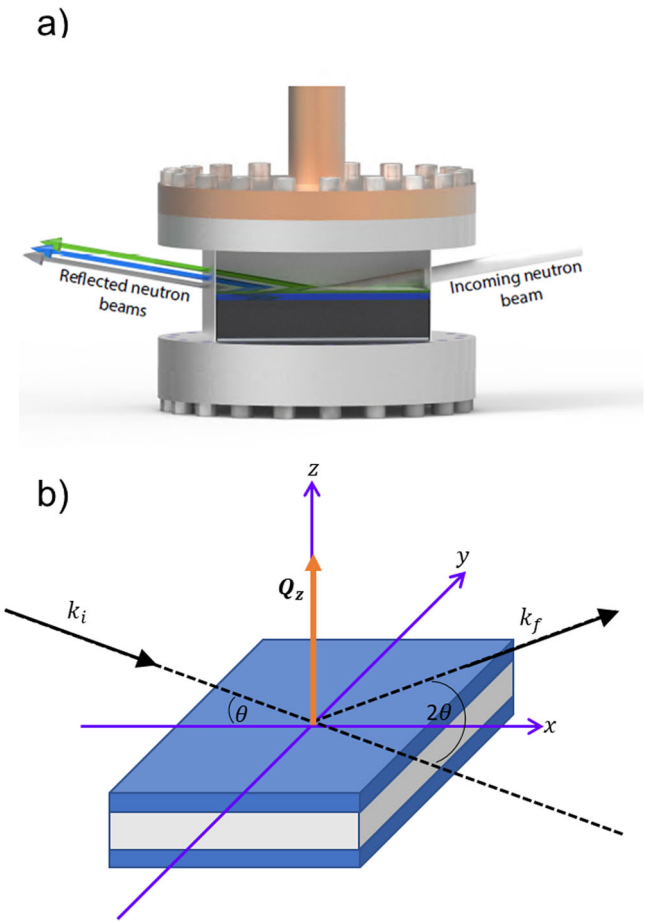

Fig. 5 | Schematic diagrams of the experimental cell and how it relates to the scattering geometry used for the study. a The position of the silicon block's surface in relation to the incoming and reflected neutron beams. **b** The scattering geometry for neutron reflection. $k_{i,f}$ are the neutron incident and final wavevector respectively. $Q_z = k_f - k_i$ is the wavevector transfer parallel to the surface normal. For off-specular scattering Q_x, the wavevector component in the plane of the sample is non-zero and information on in-plane correlations can be accessed.

distance away from the refrigerator and does not touch the equipment, save for the connecting flexible helium hose that must be attached. Care was taken to minimise the mechanical contact between other experimental necessities (such as pumping hoses and cables) and the dilution refrigerator.

The experimental cell was kept under vacuum during transport and cool-down of the dilution refrigerator, whose own automated cool-down procedure was used. Once at millikelvin temperatures, the experimental helium mixture sample itself was condensed into the experimental cell, a process that could be followed by monitoring the diagnostic and experimental thermometry data.

To condense the helium sample a bespoke gas panel was used. This allows storage of commercial ^{4}He and ^{3}He in known volumes. The gas handling equipment enables the creation of high-precision gas mixtures to ±5%. Once the mixture is made it can then be passed through a regulator at such a rate that the dilution refrigerator can condense the gas comfortably. For example, 1.15 bar-ℓ of helium mixture was condensed over 30 min, with the temperature rising to no more than 600 mK on the mixing chamber sensor.

Experimental setup

The experimental cell, shown in Fig. 4, consists of two circular copper flanges, which are indium sealed (2) to a rectangular aluminium section in between. The aluminium section has two thin-wall windows (3) for incident and scattered neutron beam access. The silicon block (4), whose surface has a high-quality finish, is placed at the bottom of the cell. We leave a 0.5 mm gap between the vertical planes of the silicon block and the aluminium walls of the cell. The single-crystal silicon substrate (4) has dimensions of 49 × 79 × 14 mm with the 111 direction polished surface normal and sits on an aluminium support block (5). The substrate is optically flat with a surface roughness of nominally 3 Å rms when purchased from the supplier. The surface is initially cleaned by UV/Ozone and subsequently cleaned in Piranha solution, this often increases the roughness to 4–6 Å rms. The sample was mounted flat to gravity such that the surface normal was parallel to gravity. Helium, condensed into the cell through the fill line (1), accumulates as bulk liquid in the bottom of the gap. This arrangement allows the formation of a saturated helium film on all exposed surfaces, including the high-quality horizontal surface of the silicon block. The distance between the bulk helium surface and the surface of the silicon block was maintained at 2.42 cm. This distance is deduced from the known volume of condensed helium mixture and the known free volume between the silicon block and the walls of the experimental cell. It is assumed that the volume of helium which makes up the film is negligibly small when compared to that of the bulk liquid. The measured film thickness of approx 160 Å is in reasonable agreement with the theoretical value of 165 Å obtained for quartz surface[52]. The upper and lower parts of the cell are shielded by cadmium foil in order to reduce secondary neutron scattering, thus reducing the background. The ruthenium-oxide sensor (7) and heater (6) are used for temperature measurement and control. The cell is attached by a copper bracket (8) to the dilution refrigerator. During the experiments, no temperature rises attributable to heating by the neutron beam have been detected.

Neutron reflectivity

As described above, the aluminium experimental cell encompasses a silicon block with a high-quality polished surface, used as the film substrate. Its geometry and position in relation to the neutron beam are illustrated in Fig. 5. The neutron beam is incident on the silicon surface at an angle θ between 0.25° and 2.0° and, after being reflected, is measured by a multi-detector[53]. The substrate sample surface was mounted horizontally. The incident beam was 30 mm wide, with the vertical height set to maintain a 60 mm long illuminated footprint at all three angles used to measure the full range of wavevector transfer, Q. This maintains a constant $\Delta Q/Q$ resolution of 1.5% and under illumination of the sample area at all times. This ensures a large area of the helium film is sampled by the neutron beam.

Two separate experiments were performed: one measuring a nominally pure ^{4}He film, and the other a ^{3}He/^{4}He mixture film. At each new temperature, we left the experimental cell for about half an hour to reach thermal equilibrium before embarking on the reflectometry measurements, which typically took several hours to complete. The sample was horizontal at all times, and an incident neutron super mirror was used to change the angle of incidence of the incoming neutron beam.

Data availability

The ISIS neutron reflectivity data are available for ISIS experiments RB1320192 and RB1910267 at the ISIS data repository. The DOIs are given in[54–57].

Received: 31 October 2023; Accepted: 31 May 2024;
Published online: 07 June 2024

References

1. D. Reinelt, J. K. & Leiderer, P. Wetting studies of liquid ^{4}He on various Cs surfaces. *J. Low Temp. Phys.* **113**, 805–810 (1998).
2. Kosterlitz, J. M. & Thouless, D. J. Ordering, metastability and phase transitions in two-dimensional systems. *J. Phys. C* **6**, 1181–1203 (1973).
3. Rollin, B. V. & Simon, F. On the "film" phenomenon of liquid helium ii. *Physica* **6**, 219–230 (1939).
4. Atkins, K. R. Third and fourth sound in liquid helium II. *Phys. Rev.* **113**, 962–965 (1959).
5. Garcia, R. & Chan, M. H. W. Critical Casimir effect near the ^{3}He-^{4}He tricritical point. *Phys. Rev. Lett.* **88**, 086101 (2002).
6. Gasparini, F. M., Kimball, M. O., Mooney, K. P. & Diaz-Avila, M. Finite-size scaling of ^{4}He at the superfluid transition. *Rev. Mod. Phys.* **80**, 1009–1059 (2008).
7. Shkarin, A. et al. Quantum optomechanics in a liquid. *Phys. Rev. Lett.* **122**, 153601 (2019).
8. Barzanjeh, S. et al. Optomechanics for quantum technologies. *Nat. Phys.* **18**, 15–24 (2022).
9. Hallock, R. B. The properties of multilayer ^{3}He-^{4}He mixture films. In (ed) Halperin, W. P. *Progress in Low Temperature Physics*, Volume 14, 321–443 (Elsevier, Amsterdam, 1995).
10. Krotscheck, E., Saarela, M. & Epstein, J. L. Impurity states in liquid-helium films. *Phys. Rev. B* **38**, 111–128 (1988).
11. Andreev, A. Surface tension of weak helium isotope solutions. *Sov. Phys. JETP* **23**, 939 (1966).
12. Ellis, F. M., Hallock, R. B., Miller, M. D. & Guyer, R. A. Phase separation in films of ^{3}He-^{4}He mixtures. *Phys. Rev. Lett.* **46**, 1461–1464 (1981).
13. Monarkha, Y. P. & Sokolov, S. S. Collective excitations in a stratified helium film. *Sov. J. Low. Temp. Phys.* **8**, 22 (1982).
14. Edwards, D. O., Shen, S. Y., Eckardt, J. R., Fatouros, P. P. & Gasparini, F. M. Propagation of surface sound in superfluid ^{3}He-^{4}He. *Phys. Rev. B* **12**, 892–904 (1975).
15. Heinrichs, R. M. & Hallock, R. B. Temperature-dependent third sound velocity measurements in ^{3}He-^{4}He films. In (ed Armitage, J. G. M.) *Helium-75*, 40–41 (World Scientific, Singapore, 1983).
16. Lurio, L. B. et al. Liquid-vapor density profile of helium: an X-ray study. *Phys. Rev. Lett.* **68**, 2628–2631 (1992).
17. Lurio, L. B. et al. Liquid-vapor density profile of helium: an X-ray study. *Phys. Rev. Lett.* **72**, 309–309 (1994).
18. Penanen, K., Fukuto, M., Silvera, I. F. & Pershan, P. S. X-ray-induced thinning of ^{3}He and ^{3}He-^{4}He mixture films. *Phys. Rev. B* **62**, 9641–9647 (2000).
19. Sivia, D. S. *Elementary Scattering Theory for X-ray and Neutron Users* (Oxford University Press, 2011). Chapter 4.
20. Lauter, H. J., Godfrin, H., Frank, V. L. P. & Leiderer, P. Ripplons in ^{4}He films observed by neutron scattering. *Phys. Rev. Lett.* **68**, 2484–2487 (1992).
21. Godfrin, H. et al. Observation of a roton collective mode in a two-dimensional Fermi liquid. *Nature* **483**, 576–579 (2012).
22. National centre for neutron research scattering length database. https://www.ncnr.nist.gov/resources/n-lengths/ (2021).
23. Dianoux, A.-J. & Lander, G. (eds) *Neutron Data Booklet* (Institut Laue-Langevin, 2002), 1st edn.
24. Lawson, C. R., Jones, A. T., Kockelmann, W., Horney, S. J. & Kirichek, O. Neutron imaging of an operational dilution refrigerator. *Sci. Rep.* **12**, 1130 (2022).
25. Godfrin, H. & Lauter, H. J. Experimental properties of ^{3}He adsorbed on graphite. In *Progress in Low Temperature Physics*, vol. 14, chap. 4, 213–320 (Elsevier, 1995).
26. Charlton, T. R. et al. Neutron reflection from a liquid helium surface. *Low. Temp. Phys.* **34**, 316 (2008).
27. Kinane, C. J., Kirichek, O., Charlton, T. R. & McClintock, P. V. E. Influence of the liquid helium meniscus on neutron reflectometry data. *Low. Temp. Phys.* **42**, 152–155 (2016).
28. Als-Nielson, J. & McMorrow, D. *Elements of Modern X-Ray Physics* (Wiley, 2001).
29. Kiessig, H. Interferenz von röntgenstrahlen an dünnen schichten. *Ann. Phys.* **402**, 769–788 (1931).
30. Kienzle, P. et al. https://www.nist.gov/ncnr/reflectometry-software (2017).
31. Yoneda, Y. Anomalous surface reflection of X rays. *Phys. Rev.* **131**, 2010–2013 (1963).
32. Cole, M. W., Frankl, D. R. & Goodstein, D. L. Probing the helium-graphite interaction. *Rev. Mod. Phys.* **53**, 199 (1981).
33. Clements, B. E., Krotscheck, E. & Saarela, M. Impurity dynamics in boson quantum films. *Phys. Rev. B* **55**, 5959–5982 (1997).
34. Sheldon, P., Vithayathil, J. P. & Hallock, R. B. Experiments to search for a substrate state for ^{3}He adjacent to surfaces in ^{3}He-^{4}He mixtures. *J. Low Temp. Phys.* **101**, 231–236 (1995).
35. Krotscheck, E. & Miller, M. D. Third sound and stability of ^{3}He–^{4}He mixture films. *J. Low Temp. Phys.* **141**, 1–25 (2005).
36. Cheng, E., Cole, M. W., Saam, W. F. & Treiner, J. Helium prewetting and nonwetting on weak-binding substrates. *Phys. Rev. Lett.* **67**, 1007–1010 (1991).
37. Bishop, D. J. & Reppy, J. D. Study of the superfluid transition in two-dimensional ^{4}He films. *Phys. Rev. B* **22**, 5171–5185 (1980).
38. Wang, X. & Gasparini, F. M. Near-monolayer ^{3}He-^{4}He films: two superfluid transitions and the ^{3}He effective mass and binding energy. *Phys. Rev. B* **38**, 11245–11258 (1988).
39. Okamura, K., Taniguchi, J., Hieda, M. & Suzuki, M. Reentrant pinning of a ^{3}He overlayer in a ^{3}He-^{4}He mixture film. *Phys. Rev. B* **100**, 214508–1–214508–5 (2019).
40. Ostermeier, R. M. & Glaberson, W. I. The mobility of ions trapped on vortex lines in pure ^{4}He and ^{3}He-^{4}He solutions. *J. Low Temp. Phys.* **25**, 317–351 (1976).
41. Senbetu, L. Effect of ^{3}He impurities on the structure of quantized vortex lines and the lifetime of negative ions trapped on vortices. *J. Low Temp. Phys.* **32**, 571–588 (1978).

42. Muirhead, C. M., Vinen, W. F. & Donnelly, R. J. The nucleation of vorticity in superfluid ^{4}He. ii. the effect of dissolved ^{3}He. *Philos. Trans. R. Soc. Lond. A* **402**, 225–243 (1985).
43. Awschalom, D. D. & Schwarz, K. W. Observation of a remanent vortex-line density in superfluid helium. *Phys. Rev. Lett.* **52**, 49–52 (1984).
44. Ankner, J. F. & Felcher, G. P. Polarized-neutron reflectometry. *J. Magn. Magn. Mater.* **200**, 741–754 (1999).
45. Majkrzak, C. F., Berk, N. F. & Perez-Salas, U. A. Phase-sensitive neutron reflectometry. *Langmuir* **19**, 7796–7810 (2003).
46. Hallock, R. B. The two-dimensional world of ^{3}He in ^{3}He-^{4}He mixture films. *J. Low. Temp. Phys.* **121**, 441–450 (2000).
47. Andreev, A. & Kompaneets, D. Gas-liquid phase transition in the system of surface impurities of ^{3}He in superfluid solutions. *JETP Lett.* **17**, 268 (1973).
48. Kirichek, O. I., Saitoh, M., Kono, K. & Williams, F. I. B. Surface fluctuations of normal and superfluid ^{3}He probed by Wigner solid dynamics. *Phys. Rev. Lett.* **86**, 4064–4067 (2001).
49. Platzman, P. M. & Dykman, M. I. Quantum computing with electrons floating on liquid helium. *Science* **284**, 1967–1969 (1999).
50. Koolstra, G., Yang, G. & Schuster, D. I. Coupling a single electron on superfluid helium to a superconducting resonator. *Nat. Commun.* **10**, 5323 (2019).
51. POLREF beamline website. https://www.isis.stfc.ac.uk/Pages/Polref.aspx (2022).
52. Cheng, E. & Cole, M. W. Retardation and many-body effects in multilayer-film adsorption. *Phys. Rev. B* **38**, 987–995 (1988).
53. Bateman, J. et al. The OSMOND detector. *Nucl. Instrum. Methods Phys. Res. A.* **698**, 168–176 (2013).
54. ISIS data DOI for experiment RB1510035 part1. https://doi.org/10.5286/ISIS.E.83550666 (2016).
55. ISIS data DOI for experiment RB1510035 part2. https://doi.org/10.5286/ISIS.E.87776553 (2017).
56. ISIS data DOI for experiment RB1510035 part3. https://doi.org/10.5286/ISIS.E.92923215 (2018).
57. ISIS data DOI for experiment RB1910267. https://doi.org/10.5286/ISIS.E.RB1910267 (2019).
58. Kerr, E. C. & Taylor, B. J. Molar volume and expansion coefficient of liquid ^{3}He. *Ann. Phys.* **20**, 450–463 (1962).
59. Kerr, E. C. & Taylor, R. D. The molar volume and expansion coefficient of liquid ^{4}He. *Ann. Phys.* **26**, 292–306 (1964).

Acknowledgements

We thank E. Krotscheck of the University at Buffalo for stimulating and helpful discussions. We are grateful to the ISIS sample environment team for supporting this experiment. Special thanks are due to R. Haynes for manufacturing the cell and C. Goodway for operating the gas handling system. We acknowledge the ISIS neutron and muon facility for the beamtime awards RB1320192 and RB1910267.

Author contributions

T.R.C. suggested the use of a silicon block as a substrate. O.K., C.R.L., C.J.K. and T.R.C. devised the experimental setup. O.K., C.R.L., C.J.K. and A.J.C. undertook the experimental measurements and analysed the data. P.V.E.Mc.C., S.L., O.K., C.R.L., A.C. and C.J.K. wrote the paper and discussed the interpretation of the results.

Competing interests

The authors declare no competing interests.

Additional information

Supplementary information The online version contains supplementary material available at https://doi.org/10.1038/s42005-024-01683-w.

Correspondence and requests for materials should be addressed to Oleg Kirichek.

Peer review information *Communications Physics* thanks the anonymous reviewers for their contribution to the peer review of this work.